Grain Boundary Carbides Evolution and Their Effects on Mechanical Properties of Ni 690 Strip Weld Metal at Elevated Temperature

Lisha Luo, Xiao Wei and Junmei Chen

Abstract Evolution of precipitates at grain boundary (GB) and their effects on mechanical properties of Ni 690 strip weld metal at elevated temperature (500–1000 °C) were studied. The precipitates at GBs were identified as $M_{23}C_6$ by energy dispersive spectroscopy (EDS) and X-ray diffraction (XRD), and the microstructure evolution and fracture surfaces were also investigated using scanning electron microscope (SEM). The morphologies of $M_{23}C_6$ carbides distributed at the GBs changed with different temperatures, including continuous carbides below 700 °C, lamellar carbides at 700 °C, and discrete carbides above 700 °C. It was found that increasing the temperature decreased the yield stress and the elongation. Lamellar carbides with 2–3 μm can cause strain concentrations at grain interior, resulting in the worse ductility of the alloy. Higher temperature above 900 °C will cause the dissolving of the carbides, making them as the source of GB cracks, hence the ductility decreased. However, there was a little increase in elongation at 800 °C due to strain concentrated at both grain interior and GB, improving the plastic deformation capacity.

Keywords Ni 690 weld metal · Elevated temperature tensile properties $M_{23}C_6$ carbides evolution · Fracture surface

1 Introduction

Alloy 690 has been widely used in nuclear power equipment for its excellent high temperature performances, and excellent resistance to stress corrosion cracking (SCC) and pitting corrosion [1–3]. The Ni-based filler metal Ni 690, as a mechanical and compositional transition material, is generally used to join the stainless steel to

L. Luo · X. Wei · J. Chen (✉)
Shanghai Key Laboratory of Materials Laser Processing and Modification, School of Materials Science and Engineering, Shanghai Jiao Tong University, 200240 Shanghai, China
e-mail: chenjm@sjtu.edu.cn

S. Chen et al. (eds.), *Transactions on Intelligent Welding Manufacturing*, Transactions on Intelligent Welding Manufacturing,
https://doi.org/10.1007/978-981-10-8740-0_4

low alloy steel in order to mitigate the residual stresses and improve the weldability of joint in nuclear power plants. During multi-pass welding, the deposition of subsequent pass changes the microstructure and mechanical properties of the underlying pass, probably causing cracks at the cooling stage. The knowledge of mechanical properties of Ni 690 weld metal at elevated temperature is an essential issue. Factors affecting mechanical properties have been studied on a wide range, including chemical compositions [4, 5], GB misorientation [6, 7], grain size [8, 9], dislocation density [8], dynamic recrystallization [10, 11] and precipitation phenomenon [12, 13]. The correlation between microstructure and high temperature mechanical properties of Ni 690 has been discussed but remains an issue with no common agreement. The micro characteristics of the weld remarkably affect the mechanical properties, and different temperature will result in different microstructure. Therefore, it is important to discuss the exact effects of microstructures, such as precipitation, on mechanical properties at elevated temperature.

Generally, $M_{23}C_6$ carbides are a commonly existed precipitate in Ni-based alloys during high temperature service [14, 15]. The existence of $M_{23}C_6$ carbides affected seriously the mechanical properties [16–19]. Mo et al. [12] investigated the effect of $M_{23}C_6$ (M = Cr, Fe) on the high temperature performance of the NiCrFe-7 weld metal made by gas tungsten arc welding (GTAW) and indicated that $M_{23}C_6$ precipitating along the GBs in the 760–980 °C range deteriorated the ductility of weld metal. However, Nissley et al. [20] inferred that $M_{23}C_6$ pinned the GBs, blocked GB migration, and improved the ductility of weld metal. The effect of $M_{23}C_6$ on elevated temperature properties of material is still a hot topic. Furthermore, Bai et al. [17] revealed that the lamellar $M_{23}C_6$ carbides formed on GBs were detrimental to an anomalous decrease in yield strength in Ni–Cr–W based superalloy at 600 °C. In addition, Hu et al. [18] investigated the tensile properties at elevated temperature in a Ni–Cr–W based superalloy and pointed out that the decreasing tensile strength and yield strength were mainly caused by the lamellar $M_{23}C_6$ carbides breaking. However, the strength of 0.3C–20Cr–11Mn–1Mo–0.35 N austenitic stainless steel was modestly improved by the precipitation of $M_{23}C_6$ carbides, as reported by Zheng et al. [19]. Bai et al. [21] also reported the discontinuous $M_{23}C_6$ carbides particles on GBs were beneficial for the improvement of tensile strength in HR3C heat-resistant steel. According to the results mentioned above, the influence of $M_{23}C_6$ carbides on the mechanical properties is related to its amount and morphology. The role of different morphologies of $M_{23}C_6$ carbides is very complex. Therefore, it is important to study the behavior of $M_{23}C_6$ carbides precipitation and its effects on the mechanical properties.

In this paper, the effect of GB $M_{23}C_6$ carbides on elevated temperature properties of Ni 690 weld metal was investigated at elevated temperature. The evolution of the amount and morphology of $M_{23}C_6$ carbides, and their effects on tensile properties had been determined and discussed in detail.

2 Experimental Procedure

Commercial Ni 690 welding strip with a dimension of 60 mm × 0.5 mm was deposited onto a low alloy steel plate using the strip cladding process. The chemical compositions of Ni 690 are provided in Table 1. There were totally three layers in the Ni 690 coating and the whole deposition thickness was 12 mm, as shown in Fig. 1. The cladding was performed with welding current of 740–760 A, welding speed of 160 mm/min and the interlayer preheating temperature of 150 °C. To avoid the effect of solute dilution on weld metal microstructures, the elevated temperature tensile specimens were extracted from the top of the strip welding layer by wire electro discharge machine. The specification of specimen was depicted in Fig. 1.

Elevated temperature tensile tests were carried out on a Zwick/Roell Z050 mechanical testing machine, with a strain rate of 5×10^{-3} s^{-1}. The testing temperatures were 500, 700, 800, 900 and 1000 °C, respectively. The specimens were heated at the rate of 20 °C/min. Before the selected temperature reached, the specimens were kept for 5 min to ensure a uniform temperature distribution. During the tensile test, the strain and the strain rate were controlled by a high-temperature extensometer, the gauge length was 15 mm. The stress-strain curve was recorded automatically.

Microstructure was analyzed by AxioCam MRc5, Carl Zeiss optical microscope (OM), JSM-7800F Scanning Electron Microscope (SEM) equipped with energy dispersive X-ray spectroscopy (EDS) microanalysis. The chemical compositions of interesting region were analyzed using the *D8 ADVANCE DA Vinci X-ray diffraction (XRD) technique. The diffraction data were collected with a step width of 0.020 and a count time of 2.0 s per step. Specimens were grounded to 2000 # sand paper, and mechanically polished, then electrolytically etched using 10% chromic acid at 4.5 V for 30 s.

Table 1 Chemical compositions of Ni 690 filler metals (weight percent)

Ni	Cr	Fe	Mn	Ti	Al	Si	C
Bal	28.91	8.79	3.99	0.20	0.16	0.26	0.03

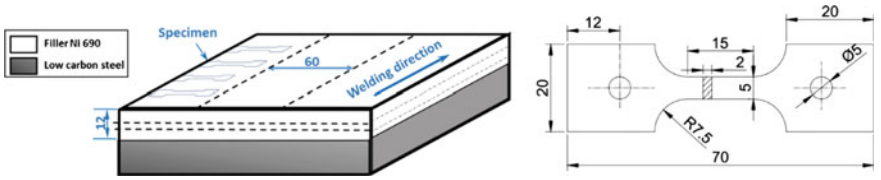

Fig. 1 Schematic illustrations of overlay and tensile test specimen

3 Results

3.1 As-Deposited Microstructure of the Alloy

Figure 2 illustrates the microstructure of the as-deposited specimens. As shown by the OM images in Fig. 2a, b, the as-deposited specimen shows an equiaxed microstructure with a grain size ranging from 200 to 600 μm. And most of the dendrites grow almost vertically to the substrate. As shown by the SEM images in Fig. 2c, d, the specimen contains lots of carbides randomly dispersed at the GBs. Previous work demonstrated that, in the multi-pass welding and deposition process, $M_{23}C_6$ carbides are sensitive to temperature and tend to precipitate at the GB. Its nucleation, growth and coarsening are aggravated by the higher temperature duration [22, 23]. To identify the GB phases, chemical compositions of these precipitates are analyzed through the EDS, the results are listed in Table 2. The GB phases are composed of two main metals: Ni and Cr. The higher content of C often existed in the Ni-base alloys [22, 23]. Furthermore, combined with XRD analytical results (Fig. 3), it indicates the probable presence of small amounts of $M_{23}C_6$. In summary, it is believed that precipitates along the GBs are $M_{23}C_6$ carbides.

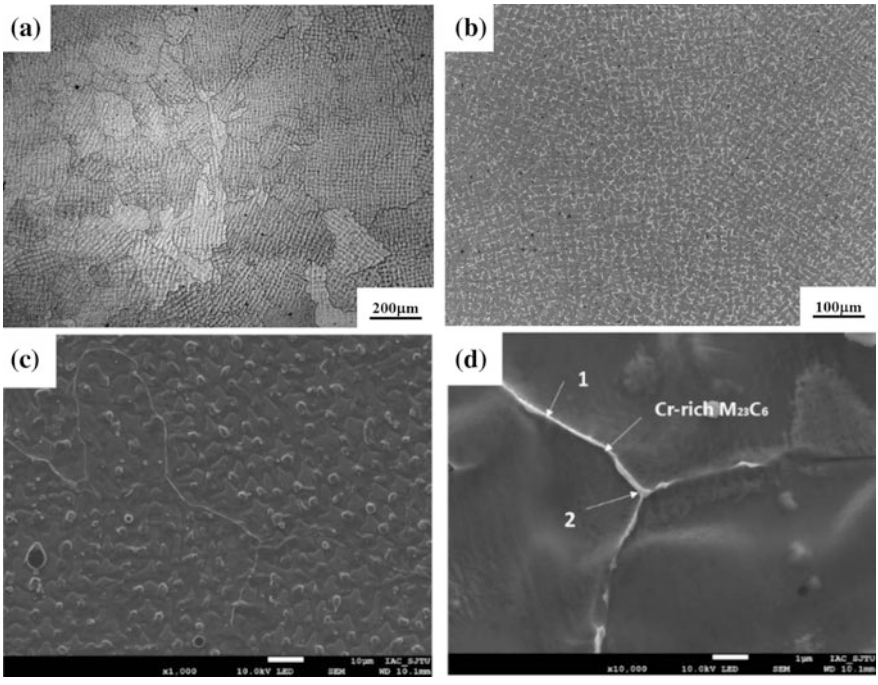

Fig. 2 Microstructure of the as-deposited specimen: **a**–**b** OM image showing an equiaxed microstructure; **c**–**d** SEM image showing the presence of GB carbides

Table 2 Chemical compositions of the precipitates and matrix (weight percent)

	C	Ti	Cr	Mn	Fe	Ni	Nb
1	6.05		30.01		10.26	52.65	1.03
2	5.22	0.2	29.46	1.43	8.91	54.78	
Matrix	0.61		30.79	4.68	9.88	54.03	

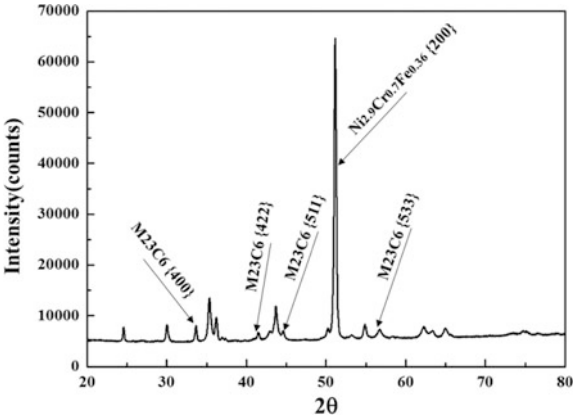

Fig. 3 XRD patterns presenting small amounts of $M_{23}C_6$ in the as-deposited specimen

3.2 *Microstructural Evolution of GB $M_{23}C_6$ Carbides at Elevated Temperature*

Figure 4 shows the morphology and distribution of GB $M_{23}C_6$ carbides after high temperature tensile tests. During heating at 500 °C, $M_{23}C_6$ carbides grow up and almost completely cover the GBs (Fig. 4a). Compared with continuous $M_{23}C_6$ carbides at 500 °C, $M_{23}C_6$ carbides with lamellar morphology are observed at 700 °C (Fig. 4b). The lamellar $M_{23}C_6$ carbides along GBs have been found in many other alloys, such as Ni-Cr-W superalloy [17, 18] and Inconel 690 [15]. While as temperature ranging from 800 to 1000 °C, some $M_{23}C_6$ carbides dissolve and others increase in size to form discrete morphology (Fig. 4c–e). It can be inferred that the solvus temperature of $M_{23}C_6$ carbides may be around 800 °C. In some Ni–Fe based alloys, similar observations on the dissolving behavior of $M_{23}C_6$ carbides at high temperatures have also been found [24]. In order to compare the changes in the amount of the GB $M_{23}C_6$ carbides, we define the fraction of $M_{23}C_6$ carbides precipitated at GBs as f_{M23C6}. The f_{M23C6} can be obtained according to its definition:

$$f_{M23C6} = \frac{l_p}{l_g}$$

where l_g is the GB length and l_p is the length of $M_{23}C_6$ carbides precipitated at GBs. Figure 4f shows the statistical result of f_{M23C6} at elevated temperature. Image *J* is

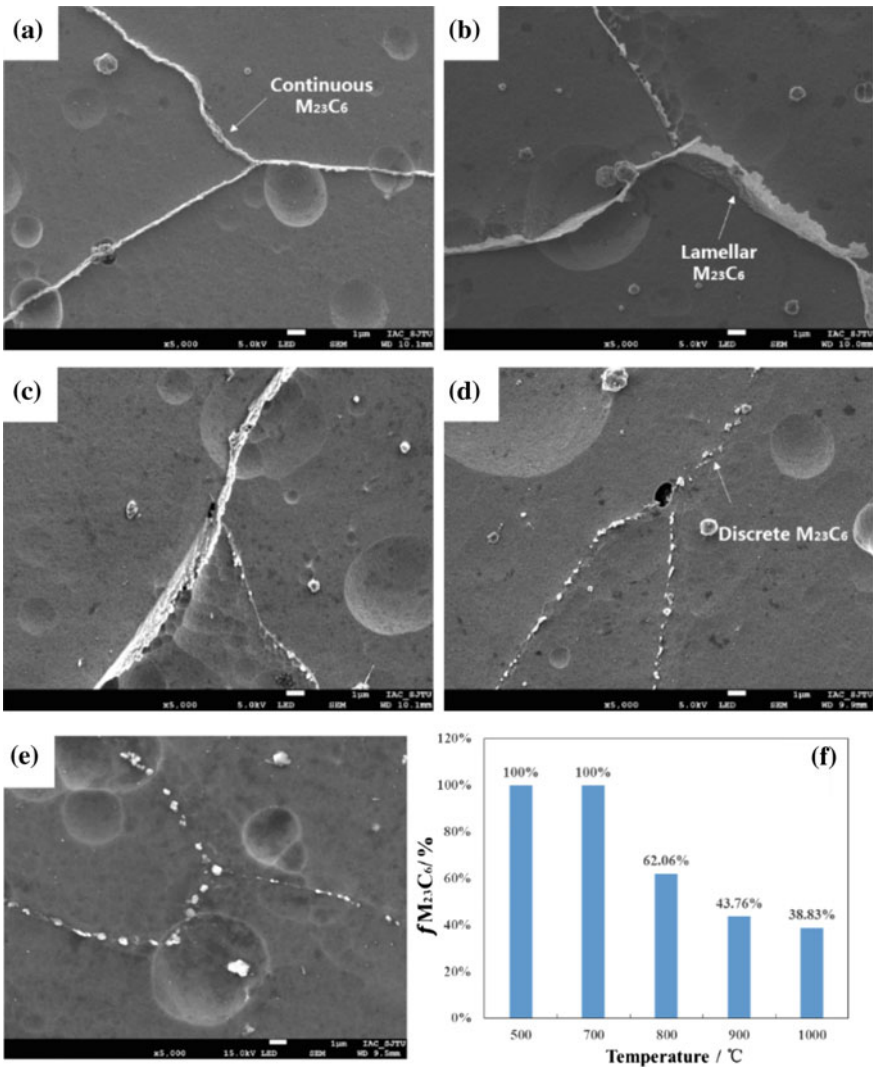

Fig. 4 The morphology of the GB $M_{23}C_6$ carbides in the specimens after the tensile test at: **a** 500 °C (continuous $M_{23}C_6$); **b** 700 °C (lamellar $M_{23}C_6$); **c** 800 °C; **d** 900 °C; **e** 1000 °C (discrete $M_{23}C_6$) and **d** f_{M23C6} at elevated temperatures

used to calculate five SEM images of $M_{23}C_6$ carbides near the fracture. It is worth noting that the amount of GB $M_{23}C_6$ carbides increases first, and then decreases from 62.06% (800 °C) to 38.83% (1000 °C).

The XRD analysis results of the specimens at 500, 700 and 900 °C are given in Fig. 5. It is demonstrated that GB $M_{23}C_6$ carbides are found. In all the diffraction patterns, the diffraction peaks of $M_{23}C_6$ at 700 °C have the highest intensity, while

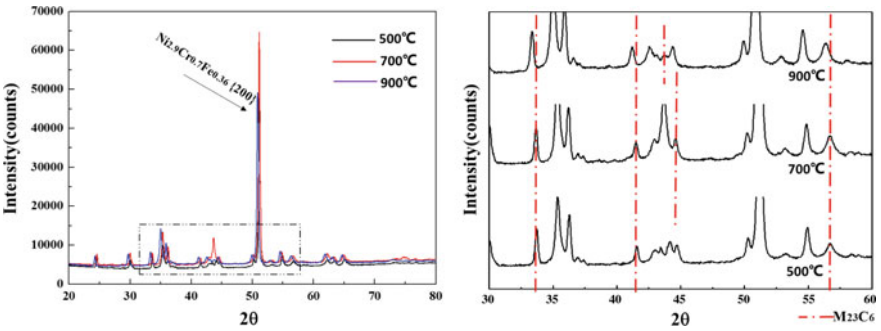

Fig. 5 Comparison of XRD patterns of the specimens at 500, 700, and 900 °C

the diffraction peaks of $M_{23}C_6$ at 900 °C are weak. Hence, these XRD results indicate that the specimens at 500 and 700 °C share the higher $M_{23}C_6$ carbides than that at 900 °C, which is consistent with the results of Fig. 5f. It can be inferred that the morphology and amount of the GB $M_{23}C_6$ carbides are associated remarkably with temperature.

3.3 Mechanical Properties at Elevated Temperatures

The stress-strain curves of the specimens at the temperature ranging from 500 to 1000 °C are shown in Fig. 6. It is found that, after yielding, the shape of stress-strain curve at 500–700 °C is very different from that at 800–1000 °C. The stress-strain curve ranging from 500 to 700 °C has a remarkable strain hardening stage and serrated flow is observed after yielding. It displays a longer extension and abrupt fracture at last. However, the stress-strain curve between 800 and 1000 °C

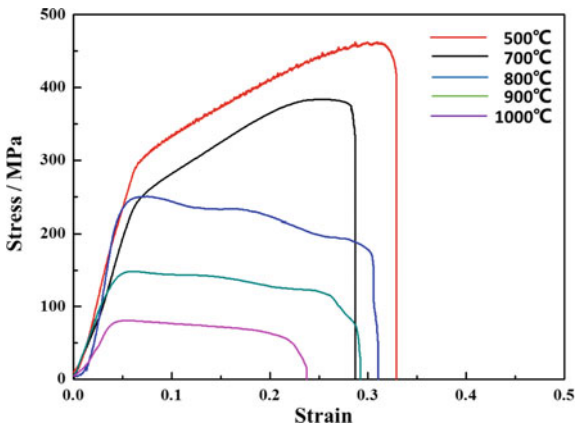

Fig. 6 Tensile stress-strain curves of the specimens at elevated temperatures

levels off after yielding and extension dimension is shorter. There is a gradual fall in stress at the end of the tensile. The specimens exhibit the loss of yield stress and ductility (elongation) as the temperature increases. The yield strength drops slightly with increasing temperature to 700 °C and drops sharply when the temperature is over 700 °C. Elongation decreases with increasing temperature to 700 °C. When the temperature is up to 800 °C, elongation increases. Then it decreases rapidly as the temperature further increases.

3.4 Fractural Characteristics

The fracture surfaces of the specimens after elevated temperature tensile test are shown in Fig. 7. It is found that the fractural mechanism turns from trans-granular fracture to inter-granular fracture as the temperature increases. Scattered dimples are observed in the fracture surfaces at temperatures of 700 °C and below, as shown in Fig. 7a, b. The fractural mode is a trans-granular mode, indicating good plastic deformation. Tearing ridges (the ligaments or intense shear bands) form between the voids and at the GBs. At 700 °C, small and shallow dimples with less density are observed on the fracture surface, as seen in Fig. 7c, d. Moreover, dimples exited at 700 °C are smaller than at 500 °C (Fig. 7a, c). The ductility of specimens further decreases with an increase in the temperature. For specimens at temperatures between 800 and 1000 °C, no dimple is observed on the fracture surface (Fig. 7e through 7i). The fractural mode is inter-granular fracture.

4 Discussion

4.1 Effects of High Temperature on $M_{23}C_6$ Carbide Precipitation

In the present study, keeping specimens at a target temperature for 5 min before tensile test is similar to a short term (1–60 min) aging treatment, which will change the number, morphology and configuration of precipitation along GBs [19]. Based on the microstructural analysis above, schematic representation of GB changes of the specimen with increasing temperature is shown in Fig. 8. The statistical results (Fig. 5f) indicate the evolution of $M_{23}C_6$ carbides in amount depends on the temperature at tensile tests, which is in agreement with the result of Refs. [16, 18]. A substitutional-diffusion controlled reaction is necessary for the formation of GB $M_{23}C_6$ carbides. This reaction occurs mainly at elevated temperatures and requires a sufficient time at low temperatures [13]. Hence, the amount of $M_{23}C_6$ carbides increases with an increase in temperature. As the temperature increases further to 800 °C, the number of nucleation sites of $M_{23}C_6$ carbides decreases. The nucleation

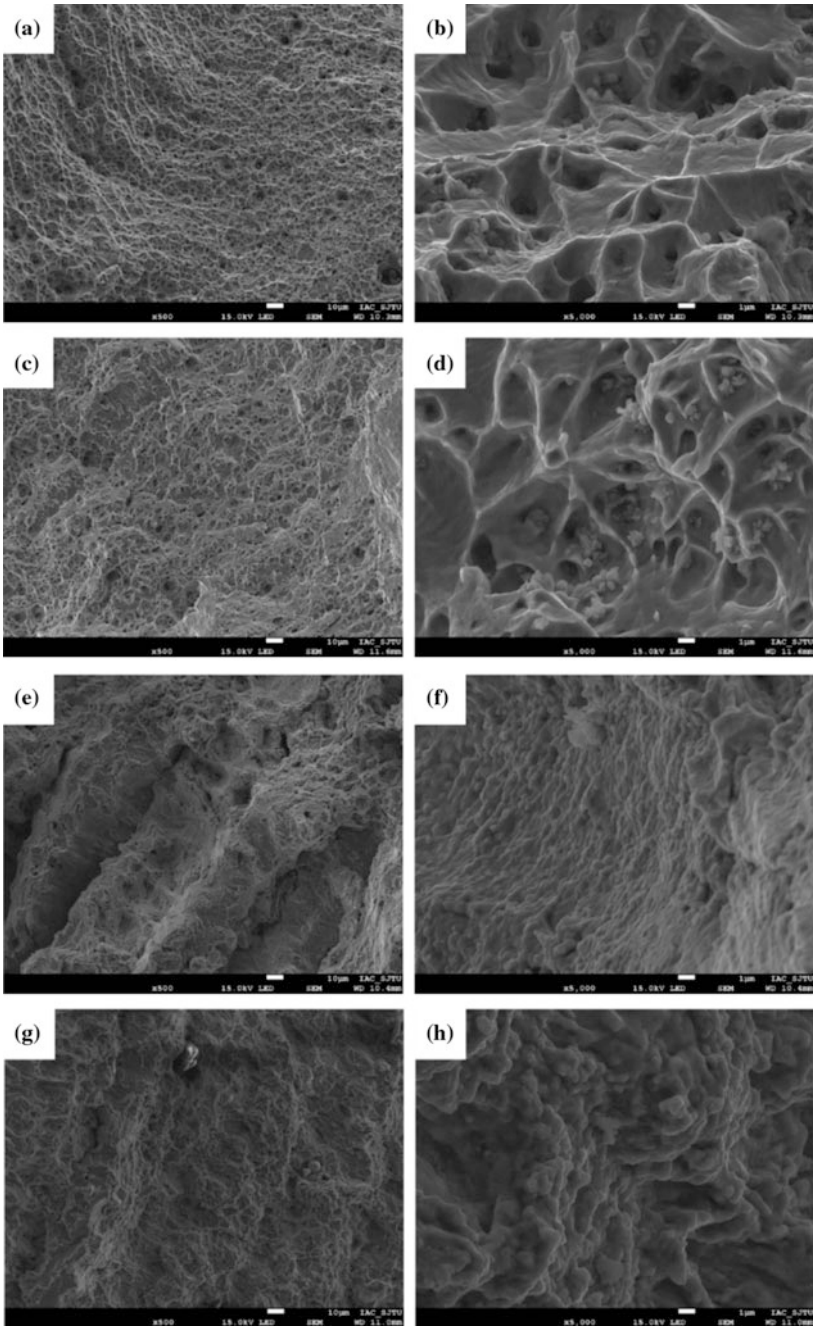

Fig. 7 The fracture of the specimen at: **a–b** 500 °C; **c–d** 700 °C; **e–f** 800 °C; **g–h** 900 °C and **i–j** 1000 °C

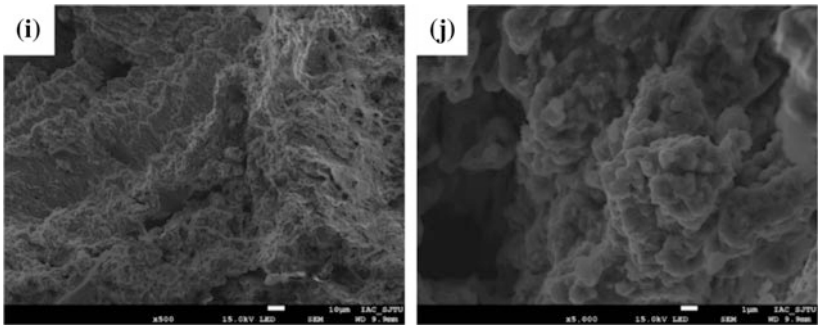

Fig. 7 (continued)

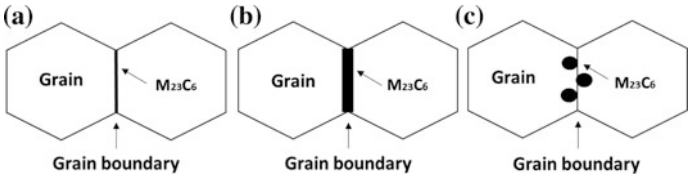

Fig. 8 Schematic representation of grain boundary changes of AR specimen during deformation process at elevated temperature: **a** continuous carbides (below 700 °C); **b** lamellar carbides (700 °C) and **c** discrete carbides (above 700 °C)

and subsequent growth of the $M_{23}C_6$ carbides become difficult at higher temperature [13]. The solid solubility of carbides increases as the temperature increases (Fig. 4c, e). Thus, the amount of $M_{23}C_6$ carbides decreases as the tensile temperature increases. As a conclusion, it can be inferred that $M_{23}C_6$ carbides are more easily to precipitate at 700 °C than other temperatures for Ni 690 weld metal during high temperature tensile test process.

4.2 Effects of $M_{23}C_6$ Carbides on High Temperature Tensile Properties

This section discusses the shifts in yield strength and ductility as well as the temperature changes in relation with the microstructure analysis.

Mechanical properties ranging from 500 to 700 °C.

In the tensile process at temperature ranging from 500 to 700 °C, both the yield strength and ductility deteriorate (Fig. 7).

The above results indicate that the variations of the tensile strength and ductility are related to the morphology and amount of $M_{23}C_6$ carbides. The morphology and amount of $M_{23}C_6$ carbides are essential to the high temperature mechanical

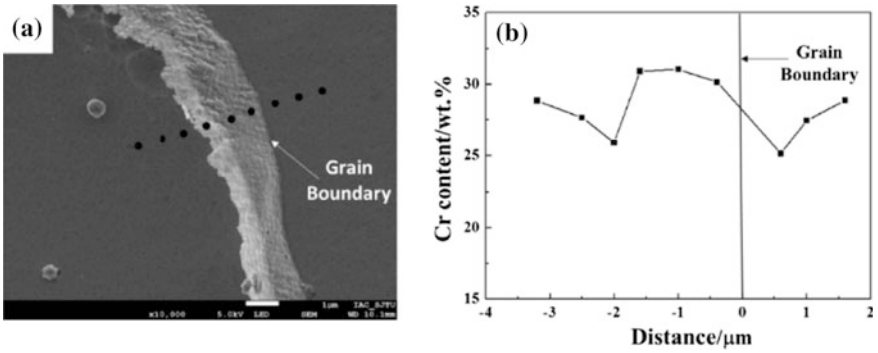

Fig. 9 SEM image after tensile test at 700 °C **a** Lamellar $M_{23}C_6$ carbides at GB; **b** The variation of Cr content across grain boundary

properties [17–19]. In this case, the concentration of Cr in matrix is lower than that in the lamellar $M_{23}C_6$ carbides. As shown in Fig. 9, the Cr concentration in front of the GB changes abruptly. When $M_{23}C_6$ carbides precipitate at the GBs, lots of Cr atoms in the matrix are consumed and bulk Cr concentration decreases. Cr element plays an important role in the strength of the alloy, and the strength decreases with decreasing Cr concentration [24, 25]. At 700 °C, the lamellar $M_{23}C_6$ carbides precipitate at GBs (Fig. 4b), the loss of Cr in matrix would cause strain concentrations at grain interior. The grain has not enough time to completely deform at that moment. It will cause initial cracks exited in the grain and expand rapidly, thus the ductility decreases accordingly. Therefore, at a low deformation temperature, the decrease in yield stress and ductility can be attributed to the precipitation of GB $M_{23}C_6$ carbides.

Mechanical properties ranging from 800 to 1000 °C.

In this stage, the yield strength continues to decrease but the ductility increases (Fig. 6). Lamellar carbides with 2–3 μm (Fig. 9) make the loss in grain interior strength which induces the abrupt fracture at 700 °C. In this case, partly lamellar carbides have transformed into discrete carbides (Fig. 4c). Cr atoms in the $M_{23}C_6$ carbides at GBs have been diffused to the matrix. So, the concentration of Cr in matrix is higher than that at 700 °C, which makes the grain interior strength recovery and the GB strength decrease. Compared to 700 °C, partial strain concentrates at the grain interior, partial strain concentrates at the GB. Therefore, the progress improves the plastic deformation capacity, and then increases the elongation to fracture.

The yield strength and ductility further decrease at 900 °C and higher temperatures. It can be seen in Fig. 10, there are many cracks exited in GBs at 900 °C. In this stage, $M_{23}C_6$ carbides dissolve in this weld metal, and small cavities initiate along the GBs (Fig. 10a). The growth and coalescence of small cavities around $M_{23}C_6$ carbides form inter-granular cracks (Fig. 10b). For the multipass welding of high Cr Ni-based alloy, Mo et al. [5, 12] and Qin et al. [22, 23] have reported that

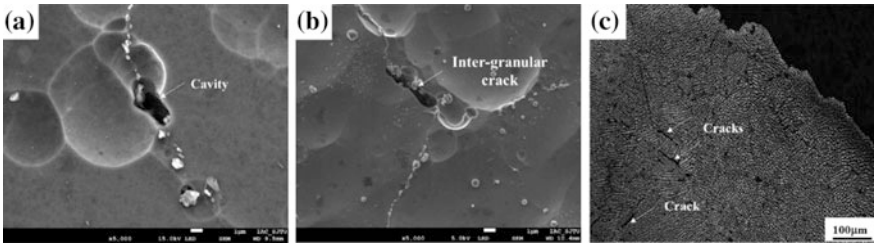

Fig. 10 SEM and optical micrograph after tensile test at 900 °C: **a** cavities at GBs and partly dissolved carbides; **b** and **c** cracks at GBs

$M_{23}C_6$ carbides deteriorate integrity of GBs and induce the local stress concentration around the GBs. The dissolving of $M_{23}C_6$ carbides will reduce the GB strength [26]. That would cause strain concentrations at GBs and then trigger the trans-granular fracture (Fig. 8). The fractural mode can reflect the relationship between the grain interior and GB strength [27]. Inter-granular fracture reveals the GB strength is lower than that of grain interior. There exit many cracks in fracture surfaces at 900 °C (Fig. 10c), which indicates the reduction in GB strength is extensive. It will trigger the fracture abrupt and result in the further decrease in ductility. The fact that the decrease in yield strength and ductility may be due to discrete GB $M_{23}C_6$ carbides, which makes the GBs relatively vulnerable and easy to cracking.

5 Conclusion

In the present study, the GB $M_{23}C_6$ carbides evolution and their effects on tensile properties of Ni 690 weld metal have been studied in details. The results are as follows:

(1) After tensile tests at 500 and 700 °C, the main changes in microstructure at GBs are precipitation and growth of $M_{23}C_6$ carbides. However, during tensile tests at 900 °C, the dissolution of $M_{23}C_6$ carbides is observed. The morphology of $M_{23}C_6$ carbides is continuous at 500 °C and has obvious changes as the temperature increases. The lamellar $M_{23}C_6$ carbides at 700 °C transform into discrete morphology, when the temperature is 900 °C. Moreover, the amount of $M_{23}C_6$ carbides first increase, and then decreases with increasing temperature.
(2) The stress-strain curve of specimens at temperatures of 700 °C and below has a remarkable strain hardening stage, however, the stress gradually decreases as the deformation proceed after yielding for specimens at 800–1000 °C. Temperature has only small influence on modulus of elasticity but has a much higher influence on ductility and strength. The yield strength reduces gradually

with the increasing of temperature. However, the ductility first decreases and then increases with increasing temperature to 800 °C, while it decreases gradually when the temperature further increases.

(3) There exit some dimples at fracture surfaces and the fracture mode is a trans-granular mode, during heating at 500 and 700 °C. The precipitation of $M_{23}C_6$ carbides at GBs is the main factor that deteriorates the strength and ductility of weld metal. When the temperatures are over 700 °C, the fractural mode is inter-granular. At 800 °C, deformation is concentrated at the grain interior, and the GB. It improves the plastic deformation capacity and increases the elongation to fracture. At 900 °C and higher temperatures, the dissolving of $M_{23}C_6$ carbides reduces the GB strength, which results in the further decrease in ductility.

Acknowledgements This research was supported by the National Natural Science Foundation of China (51204107 and 51575347).

References

1. Kai JJ, Yu GP, Tsai CH et al (1989) The effects of heat treatment on the chromium depletion, precipitate evolution, and corrosion resistance of INCONEL alloy 690. Metall Mater Trans A 20:2057–2067
2. Young BA, Gao X, Srivatsan TS et al (2007) The response of alloy 690 tubing in a pressurized water reactor environment. Mater Des 28:373–379
3. Andresen PL, Morra MM (2008) Stress corrosion cracking of stainless steels and nickel alloys in high-temperature water. Corrosion 64:15–29
4. Jeng SL, Chang YH (2012) The influence of Nb and Mo on the microstructure and mechanical properties of Ni–Cr–Fe GTAW welds. Mater Sci Eng, A 555:1–12
5. Mo W, Lu S, Li D et al (2013) Effects of filler metal composition on the microstructure and mechanical properties for ER NiCrFe-7 multi-pass weldments. Mater Sci Eng, A 582:326–337
6. Ramirez AJ, Lippold JC (2004) High temperature behavior of Ni-base weld metal: part II–Insight into the mechanism for ductility dip cracking. Mater Sci Eng, A 380:245–258
7. Lim YS, Kim DJ, Hwang SS et al (2014) $M_{23}C_6$ precipitation behavior and grain boundary serration in Ni-based Alloy 690. Mater Charact 96:28–39
8. Diano P, Muggeo A, van Duysen JC (1989) Relationship between microstructure and mechanical properties of alloy 690 tubes for steam generators. J Nucl Mater 168:290–294
9. Blaizot J, Chaise T, Nélias D et al (2016) Constitutive model for nickel alloy 690 (Inconel 690) at various strain rates and temperatures. Int J Plast 80:139–153
10. Li KK, Chen MS, Lin YC et al (2016) Microstructural evolution of an aged Ni-based superalloy under two-stage hot compression with different strain rates. Mater Des 111:344–352
11. Chen MS, Li KK, Lin YC et al (2016) An improved kinetics model to describe dynamic recrystallization behavior under inconstant deformation conditions. J Mater Res 31:2994–3003
12. Mo W, Lu S, Li D et al (2014) Effects of $M_{23}C_6$ on the high-temperature performance of Ni-based welding material NiCrFe-7. Metall Mater Trans A 45:5114–5126
13. Lee TH, Suh HY, Han SK et al (2016) Effect of a heat treatment on the precipitation behavior and tensile properties of alloy 690 steam generator tubes. J Nucl Mater 479:85–92

14. Angeliu TM, Was GS (1990) Behavior of grain boundary chemistry and precipitates upon thermal treatment of controlled purity alloy 690. Metall Mater Trans A 21:2097–2107
15. Lim YS, Kim JS, Kim HP et al (2004) The effect of grain boundary misorientation on the intergranular $M_{23}C_6$ carbide precipitation in thermally treated Alloy 690. J Nucl Mater 335:108–114
16. He LZ, Zheng Q, Sun XF et al (2005) $M_{23}C_6$ precipitation behavior in a Ni-base superalloy M963. J Mater Sci 40:2959–2964
17. Bai G, Li J, Hu R et al (2011) Effect of temperature on tensile behavior of Ni–Cr–W based superalloy. Mater Sci Eng, A 528:1974–1978
18. Hu R, Bai G, Li J et al (2012) Precipitation behavior of grain boundary $M_{23}C_6$ and its effect on tensile properties of Ni–Cr–W based superalloy. Mater Sci Eng, A 548:83–88
19. Zheng L, Hu X, Kang X et al (2015) Precipitation of $M_{23}C_6$ and its effect on tensile properties of 0.3C–20Cr–11Mn–1Mo–0.35 N steel. Mater Des 78:42–50
20. Nissley NE, Lippold JC (2009) Ductility-dip cracking susceptibility of nickel-based weld metals: part 2—microstructural characterization. Weld J 88:131–140
21. Bai X, Pan J, Chen G et al (2014) Effect of high temperature aging on microstructure and mechanical properties of HR3C heat resistant steel. Mater Sci Technol 30:205–210
22. Qin R, Duan Z, He G (2013) Microstructure and ductility-dip cracking susceptibility of circumferential multipass dissimilar weld between 20MND5 and Z2CND18-12NS with Ni-base filler metal 52. Metall Mater Trans A 44:4661–4670
23. Qin R, Wang H, He G (2014) Investigation on the microstructure and ductility-dip cracking susceptibility of the butt weld welded with ENiCrFe-7 nickel-base alloy-covered electrodes. Metall Mater Trans A 46:1227–1236
24. Zhong Z, Gu Y, Yuan Y (2015) Microstructural stability and mechanical properties of a newly developed Ni–Fe-base superalloy. Mater Sci Eng, A 622:101–107
25. Jiao SY, Zhang MC, Zheng L et al (2010) Investigation of carbide precipitation process and chromium depletion during thermal treatment of Alloy 690. Metall Mater Trans A 41:26–42
26. Wei X, Xu M, Wang Q et al (2010) Effect of local texture and precipitation on the ductility dip cracking of ERNiCrFe-7A Ni-based overlay. Mater Des 110:90–98
27. Horikawa K, Kuramoto S, Kanno M (2001) Intergranular fracture caused by trace impurities in an Al–5.5 mol% Mg alloy. Acta Mater 49:3981–3989